Absolute configuration assignment of highly fluorinated carboxylic acids via VCD and MRR spectroscopy

Absolute configuration assignment of highly fluorinated carboxylic acids via VCD and MRR spectroscopy

Dimitri J.S. De Waele[a,†], Sjobbe Luyten[a,†], Reilly E. Sonstrom[b], Jonathan Bogaerts[a], Justin L. Neill[b], Peter Viereck[c], Karel Goossens[d], Mattijs Baeten[d], Nico Vervoort[d], Wouter Herrebout*[,a]

[a] Department of Chemistry, University of Antwerp, Groenenborgerlaan 171, B-2020, Antwerp, Belgium.

[b] BrightSpec, Inc., 770 Harris Street Suite 104b, Charlottesville, Virginia 22903, United States

[c] Chemical Process R&D, Discovery Process Research, Janssen R&D Turnhoutseweg 30, B-2340 Beerse, Belgium.

[d] Chemical Process R&D, Process Analytical Research, Janssen R&D, Turnhoutseweg 30, B-2340, Beerse, Belgium.

[†] Authors contributed equally.

Correspondence:

Prof. dr. Wouter Herrebout.

Address: Department of Chemistry, University of Antwerp, Groenenborgerlaan 171, B-2020, Antwerp, Belgium.

E-mail: wouter.herrebout@uantwerpen.be

Graphical Abstract

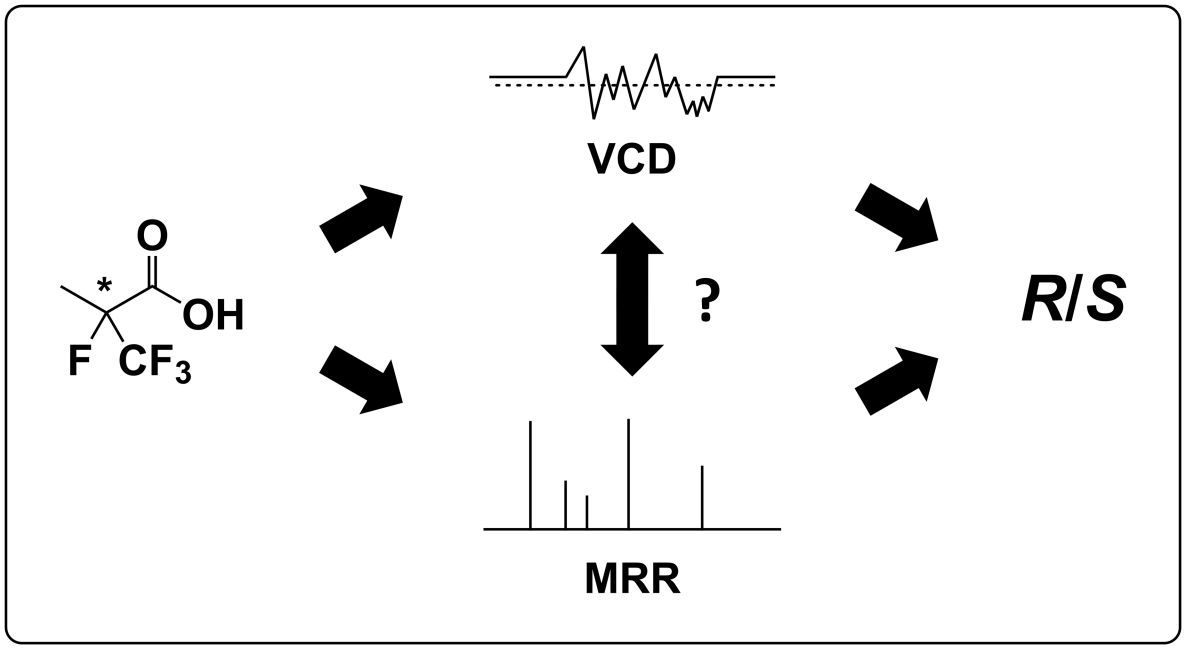

The AC of two highly fluorinated carboxylic acids were successfully assigned using VCD and MRR spectroscopy. The comparative study demonstrates the power of contemporary VCD analysis and the unique contributions of MRR to the analytical toolbox.

Abstract

Chiral analysis has become a crucial step in studying the stereospecific synthesis of Active Pharmaceutical Ingredients (APIs). Both Vibrational Circular Dichroism (VCD) and Molecular Rotational Resonance (MRR) spectroscopy are capable of determining absolute configurations (ACs) via comparison of experimental and calculated data. In this regard, each technique has its own caveats. In VCD analysis, accurate prediction of the normal modes as well as rigorous conformational searches of both the analyte and potential (self-)aggregation products are required to optimally match experimental spectra. In MRR analysis, chiral species are resolved through complexation with a chiral tag to prepare spectrally distinct diastereomeric complexes. Although individual complex isomers can be distinguished, spectral assignments need to be matched to unique isomer geometries for unambiguous AC assignment. In this work, the ACs of two highly fluorinated carboxylic acids were successfully assigned using VCD and MRR spectroscopy. In the VCD analysis, the M06-2X functional was demonstrated to be superior to B3LYP and B3LYP-GD3 in accurately predicting the C–F normal modes and both monomeric and dimeric spectral contributions were observed. In a similar analysis with broadband MRR, most experimentally identified geometries had more than one possible computational match. Nevertheless, careful consideration of the chiral tag, as well as additional isomer assignments, resulted in successful assignment of the AC. This comparative study demonstrates the power of contemporary VCD analysis and the unique contributions of MRR to the analytical toolbox.

Keywords: chiral analysis, rotational spectroscopy, absolute configuration, microwave spectroscopy, molecular rotational resonance, vibrational circular dichroism, carboxylic acids

1 Introduction

Most contemporary Active Pharmaceutical Ingredients (APIs) possess one or more chiral centers and are synthesized through a meticulous multistep process.[1, 2] In recent years, advances in asymmetric catalysis have revolutionized stereospecific synthesis within the pharmaceutical industry by accelerating the search for optimal reaction conditions towards the desired stereoisomer in each individual step, which necessitates unambiguous assignment of the absolute configuration (AC) of each intermediate formed.[3] Although chromatography-based techniques, often hyphenated with mass spectrometry (MS), remain the gold standard as an analytical tool, they cannot be used to assign AC without the use of a reference standard. Hence, other analytical techniques need to be used to assign the AC of each intermediate, examples of which are: X-Ray Diffraction (XRD)[4-7], Electronic Circular Dichroism (ECD)[6, 8], Optical Rotation (OR)[9], and even Nuclear Magnetic Resonance (NMR).[10] However, each of these techniques suffers from inherent drawbacks: XRD can only be performed on solids, requires the production of a high-quality single crystal, and may not represent the AC of the bulk material[4-7]; ECD is only possible when chromophores are present in the analyte[6, 8]; OR can only reliably determine the AC through calibration using a sample of known AC[9]; and NMR requires derivatization with a chiral derivatization agent (CDA), for instance to a so-called Mosher ester,[10, 11] or the use of a chiral solvating agent (CSA).

Vibrational Optical Activity (VOA) techniques, consisting of Vibrational Circular Dichroism (VCD) and Raman Optical Activity (ROA), can be used for AC determination as well.[12-16] Indeed, VCD spectroscopy, the chiral extension of infrared (IR) spectroscopy where the vibrational states of the molecule are probed with the added sensitivity to chirality, has established itself over the last decades as one of the most powerful tools to assign the AC of small synthetic molecules and natural products alike, directly in solution and without the need for derivatization or crystallization.[17-19] However, VCD signals have an inherently low intensity (about 4–5 orders of magnitude smaller than the parent IR signals), leading to increased measurement times to obtain a sufficient signal-to-noise ratio.[17]

In the past few years, Molecular Rotational Resonance (MRR) spectroscopy has emerged as another technique for determination of the AC of small molecules in the gas phase.[20-23] MRR, also known in the literature as rotational spectroscopy, identifies molecules through the experimental determination of their principal moments of inertia, which are represented through the rotational constants.[24] Although rotational spectroscopy is intrinsically insensitive to chirality, as enantiomers have the same moments of inertia, pulsed supersonic expansion sources can generate non-covalent complexes. Consequently, chiral tag compounds can convert spectroscopically equivalent enantiomers into diastereomeric complexes in the gas phase that can be resolved.[20, 22, 25-27] Thanks to

the move in recent years from slow narrowband scanning spectrometers[28, 29] to broadband spectrometers that can simultaneously characterize all of the volatile components in a sample,[30] the measurement of these chiral tag complexes has become experimentally practical. The development of new dispersion-corrected density functional theory (DFT-D) methods has enabled the accurate prediction of complex structures, as well as the relative energies of the different conformers and isomers that can occur.[31-34] With these improvements, several recent studies have laid out how both AC and enantiomeric excess can be accurately determined with this method.[20, 35, 36] The inherently high resolution of the technique and possibility to measure a reaction mixture without purification have sparked a renewed interest in rotational spectroscopy as a process analytical tool.[35, 37-39] Similar to VCD, MRR spectroscopy is capable of assigning AC without the need for reference material, provided a comparison with quantum-chemical calculations can be made.[17, 18, 20, 40]

Side-by-side studies of spectroscopic techniques are rather scarce in literature. We present here a study exploring the ability of VCD and broadband MRR to determine the AC of two highly fluorinated carboxylic acids, namely (*R*)- and (*S*)-2,3,3-trifluoro-2-methylpropanoic acid (**1**) and (*R*)- and (*S*)-2,3,3,3-tetrafluoro-2-methylpropanoic acid (**2**) (Figure 1).

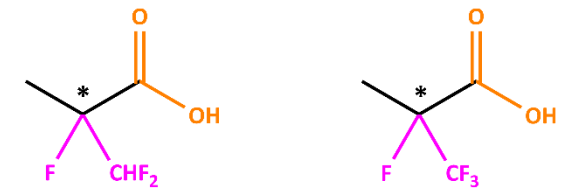

2,3,3-trifluoro-2-methylpropanoic acid (compounds **1A** and **1B**)

2,3,3,3-tetrafluoro-2-methylpropanoic acid (compounds **2A** and **2B**)

Figure 1. The structures of the two highly fluorinated carboxylic acids that were studied in this work using vibrational (VCD) and rotational (broadband MRR) spectroscopy.

These compounds represent model systems for fluorinated drugs built upon a carboxylic acid scaffold, the relevance of which is highlighted by the *Top 200 Pharmaceuticals by Retail Sales in 2022* list composed by McGrath *et al*.[41, 42]

Carboxylic acids are polar entities, which are known to pose challenges in VCD analysis when polar solvents such as CD_3CN, CD_3OD or DMSO-d_6 are used.[43, 44] For AC determination of carboxylic acids via VCD, it is therefore advisable to use apolar solvents such as $CDCl_3$ whenever possible to avoid having to take explicit solvent effects into consideration during calculations. However, because carboxylic acids are prone to self-aggregation in apolar solvents[45, 46], it is necessary to account for both monomer and dimer conformations, which increases the complexity and time cost of the VCD analysis. The highly fluorinated nature of the analytes **1** and **2** must be kept in mind as well. Hybrid functionals commonly used for VCD calculations, such as B3LYP[47-51] and B3PW91[51-56], have been demonstrated to commonly

misplace C−F asymmetric and symmetric stretching vibrations.[57] Therefore, in this work, the less commonly used M06-2X[58] functional was used, which was shown by Kreienborg *et al*. to more accurately predict these C−F normal modes.[57] Compounds **1** and **2** feature both a carboxylic acid moiety and an interesting fluorination pattern and are therefore excellent examples for demonstrating how VCD and MRR approach AC determination differently. This work does not aim to perform a full spectroscopic analysis of the experimental data, but rather evaluate the ability of these spectroscopies to quickly and unambiguously elucidate the AC of chiral building blocks, synthetic intermediates and APIs within an industrial context. As such, we present the vibrational and rotational determination of the AC configuration of **1** and **2** independently of each other.

2 Materials and methods

2.1 Materials

Enantiopure samples of 2,3,3-trifluoro-2-methylpropanoic acid (compounds **1A** and **1B**) and 2,3,3,3-tetrafluoro-2-methylpropanoic acid (compounds **2A** and **2B**) were provided by Janssen Pharmaceutica NV (Belgium) and used without further purification. Deuterated chloroform ($CDCl_3$, 99.8 atom% D) was purchased from Sigma-Aldrich (Germany). Research-grade (>99.999%) neon was used as the carrier gas for MRR analysis. Propylene oxide (racemic and enantiopure) was purchased from TCI America (U.S.A.); both samples had chemical purity >98%. 1,1,1-Trifluoropropan-2-ol (racemic and enantiopure) was purchased from Synquest Labs (U.S.A.); both samples had chemical purity >97%. All tag samples were used without further purification.

2.2 Experimental methods

2.2.1 Vibrational spectroscopy measurements

IR and VCD measurements of **1** and **2** were carried out on a dual PEM ChiralIR-2X spectrometer (BioTools, Inc.). Solutions of **1** and **2** in $CDCl_3$ were held in a transmission cell with BaF_2 windows and a path length of 100 µm, at a concentration of 0.12 M. Both the IR and the VCD spectra were recorded at a spectral resolution of 4 cm^{-1} by accumulating 72000 scans over a period of 24 h. Baseline-corrected VCD spectra were obtained via the virtual racemate. In this procedure, the experimental VCD spectrum is displayed as half the difference between the enantiomeric VCD spectra. Consequently, the IR spectrum is presented as half the sum of the enantiomeric IR spectra.

2.2.2 Rotational spectroscopy measurements

Broadband MRR measurements were carried out on a chirped-pulse Fourier transform microwave (CP-FTMW) spectrometer (BrightSpec, Inc.) operating in the 2–8 GHz frequency range. Pure **1** and **2** were sufficiently volatile at room temperature to generate enough vapor pressure for analysis without sample heating. Neon carrier gas was used at a backing pressure of 10-15 psi, pre-mixed with the chiral tag sample of interest at a concentration of 0.1% by volume. The compounds were volatilized and introduced into the vacuum chamber of the spectrometer, held at $<10^{-5}$ Torr, through three simultaneously operating supersonic expansion nozzles (Parker Series 9). The rotational temperature of the compounds and complexes observed in the resulting spectra was approximately 1 K. Individual measurements were performed over a period of approximately 1.4–4.6 hrs.

2.3 Computational methods

For both VCD and MRR, there are no empirical methods to determine the AC directly from experimental VCD and MRR spectra. To assign the AC, a conformational analysis followed by quantum-chemical calculations starting from a structure of known AC were performed to produce simulated data which could be compared to the experimental data. In VCD, the spectral pattern is a Boltzmann average of individual conformers, so it is crucial to find all relevant conformers. In MRR, individual complex isomers can be distinguished, hence only the low-energy isomers need to be identified in the spectrum. For MRR, the geometry of the chiral tag complex is needed for AC, so the conformational analysis must be performed separately for the two techniques. Additionally, VCD and MRR are sensitive to different aspects of the molecule's structure, and so different quantum chemical methods are used for the final geometry optimizations.

2.3.1 Vibrational spectroscopy calculations

First, a conformational analysis on the (*R*)-monomers of **1** and **2** was performed in PCModel 10.07[59] using the MMFF94[60] force field at an energy cut-off of 5 kcal mol^{-1}. The identified conformations were further optimized via DFT, as implemented in Gaussian 16[61], at the M06-2X[58, 62] / 6-311++G(2d,p)[63-67] level of theory, using tight convergence criteria and ultrafine integration grids. Each of the optimized monomer conformations having a *cis* configuration in the carboxylic moiety (whereby the acidic H is *cis*-positioned with respect to the carbonyl O) were mutually combined to manually produce the corresponding (*R*,*R*)-dimer complexes. These dimer complex conformations were further optimized at the M06-2X / 6-311++G(2d,p) level of theory, again using tight convergence criteria and ultrafine integration grids. In all cases, the self-consistent reaction field (SCRF) approach via the integral

equation formalism polarizable continuum model (IEFPCM)[68-70] was used to include the $CDCl_3$ solvent. The calculated IR and VCD monomer and dimer line spectra were broadened using a Lorentzian function with a full-width-at-half-maximum (FWHM) of 12 cm^{-1} and Boltzmann-weighted using the enthalpy-corrected relative energies ($\Delta H°$) to yield the final monomer and dimer spectra. A frequency scaling factor of 0.967 and 0.975 was applied for **1** and **2**, respectively, as determined by maximizing the overlap integral[71] between the experimental and calculated monomer VCD spectra in the wavenumber range 950–1600 cm^{-1}. In all calculations, enthalpy-corrected relative energies ($\Delta H°$) are preferred over Free Energy-corrected relative energies ($\Delta G°$) , as they are generally accepted to result in more reliable Boltzmann weights.[16] The level of agreement between experimental and theoretical spectra is quantified by calculating the appropriate overlap integrals.[16,17] These integrals typically vary between 0 (0%) and 1 (100%) for IR, and between -1 (-100%) and +1 (100%) for VCD, but do not reflect possible errors in determining the AC using VCD.

2.3.2 Rotational spectroscopy calculations

The following set of diastereomeric complexes, homochiral and heterochiral, were constructed for conformational analysis using CREST[32]: **1**/PO, **2**/PO, and **2**/TFIP. The terms heterochiral and homochiral refer to the relative stereochemistry of the chiral tag and analyte based on the Cahn-Ingold-Prelog naming convention. CREST[32] calculations were performed using the default energy window of 6 kcal mol^{-1}. The resulting conformers were reordered using single-point energies calculated at the B3LYP-GD3BJ / 6-311++G(d,p) level of theory. Next, all conformers within an energy window of 600 cm^{-1} were further optimized at the B3LYP-GD3BJ / def2-TZVP[33, 64, 65, 67] level of theory. A summary of the quantum-chemical calculations and related structures can be found in the electronic supplementary information (ESI).

3 Results and discussion

3.1 Vibrational analysis

In the case of compound **1**, the conformational search with subsequent optimization at the M06-2X / 6-311++G(2d,p) level of theory yielded nine unique conformations of the (*R*)-monomer (m). The torsional angles α, β and γ, associated enthalpy-corrected energies ($\Delta H°$) as referenced to *H*(**1**-m1), and corresponding Boltzmann populations (pop.) of the **1** (*R*)-monomer conformers are summarized in Table 1.

Table 1: The torsional angles α, β and γ, associated enthalpy-corrected energies (*ΔH°*), and corresponding Boltzmann populations (pop.) of the nine unique conformations of the **1** (*R*)-monomer (m), calculated at the M06-2X / 6-311++G(2d,p) / SCRF($CHCl_3$) level of theory.

Monomer	α (°)[a]	β (°)[a]	γ (°)[a]	*ΔH°* (kcal mol^{-1})[b]	Pop. (*ΔH°*) (%)
1-m1	71.98	0.19	58.93	0.00	24.3
1-m2	-109.15	-0.46	64.43	0.07	21.6
1-m3	62.74	178.15	60.20	0.15	19.0
1-m4	-115.90	-1.44	-162.81	0.49	10.6
1-m5	11.01	-0.45	-63.08	0.67	7.9
1-m6	49.08	0.38	-169.16	0.77	6.7
1-m7	-146.53	-1.46	-59.72	0.91	5.3
1-m8	50.50	-179.60	-169.41	1.12	3.7
1-m9	56.37	-178.61	-55.38	1.88	1.0

[a] α = (C_{CH3}–C_{α}–C=O), β = (O=C–O–H) and γ = (H–C_{CHF2}–C_{α}–C_{COOH}). [b] Referenced to *H*(**1**-m1) = -605.312986 Hartree.

The dihedral angle α describes the angle between the methyl carbon, the alpha carbon, the carbonyl carbon and the carbonyl oxygen (C_{CH3}–C_{α}–C=O). The dihedral angle β (O=C–O–H) describes either a *cis* (β = 0°) or *trans* (β = ±180°) configuration of the carboxylic acid group. The dihedral angle γ describes the angle between the hydrogen atom of the –CHF_2 group, the carbon atom of the –CHF_2 group, the alpha carbon atom and the carbonyl carbon atom (H–C_{CHF2}–C_{α}–C_{COOH}). Six of the nine low-energy monomer conformers display a *cis* configuration in the –COOH group, as described by β (Table 1), resulting in the formation of 21 (*R*,*R*)-dimer (d) complexes. The torsional angles α, β and γ, associated enthalpy-corrected energies (*ΔH°*) as referenced to *H*(**1**-d22), and corresponding Boltzmann populations (pop.) of the **1** dimer conformers are summarized in Table 2. Here, **1**-d12 denotes a dimer of compound **1** constructed from monomer conformer subunits **1**-m1 and **1**-m2. The dihedral angles α_1 and α_2 and γ_1 and γ_2 describe the α and γ angles of subunits 1 and 2, respectively. The lowest energy conformers of the **1** monomer (left) and dimer (right) are shown in Figure 2.

Table 2: The torsional angles α_1 and γ_1 of monomer subunit 1, α_2 and γ_2 of monomer subunit 2, associated enthalpy-corrected energies (*ΔH°*), and corresponding Boltzmann populations (pop.) of the 21 unique conformations of the **1** dimer (dxy denotes a dimer consisting of monomer subunit 1 conformer x and monomer subunit 2 conformer y), calculated at the M06-2X / 6-311++G(2d,p) / SCRF($CHCl_3$) level of theory.

Dimer	α_1 (°)[a]	γ_1 (°)[a]	α_2 (°)[a]	γ_2 (°)[a]	*ΔH°* (kcal mol^{-1})[b]	Pop. (*ΔH°*) (%)
1-d22	-111.22	63.74	-111.22	63.74	0.00	18.1
1-d12	73.00	60.41	-108.24	63.63	0.07	16.0
1-d11	69.38	60.11	69.38	60.11	0.14	14.3
1-d14	71.64	60.05	-120.34	-163.84	0.51	7.7
1-d24	-110.21	63.50	-120.17	-164.12	0.57	7.0
1-d26	-108.55	63.49	55.11	-167.66	0.64	6.2
1-d16	69.15	60.03	52.84	-167.69	0.84	4.4
1-d25	-109.75	63.65	15.72	-63.11	0.90	3.9
1-d15	70.96	60.18	14.82	-62.74	1.00	3.3
1-d27	-110.14	63.83	-149.23	-60.75	1.04	3.2

1-d17	71.47	60.06	-146.90	-60.67	1.14	2.7
1-d44	-118.03	-163.70	-118.89	-163.77	1.16	2.6
1-d64	52.83	-167.53	-119.14	-163.78	1.23	2.3
1-d54	13.29	-63.07	-118.63	-163.57	1.41	1.7
1-d74	-149.49	-60.36	-119.51	-163.85	1.55	1.3
1-d66	52.89	-167.66	52.89	-167.66	1.56	1.3
1-d56	15.06	-62.53	52.76	-168.02	1.63	1.2
1-d76	-149.28	-60.66	54.13	-167.93	1.75	0.9
1-d55	12.38	-63.17	12.38	-63.17	1.87	0.8
1-d57	13.79	-62.86	-151.82	-60.84	1.95	0.7
1-d77	-147.21	-60.72	-147.22	-60.72	2.04	0.6

[a] $\alpha_1 = \alpha_2 = (C_{CH3}{-}C_{\alpha}{-}C{=}O)$ and $\gamma_1 = \gamma_2 = (H{-}C_{CHF2}{-}C_{\alpha}{-}C_{COOH})$. [b] Referenced to *H*(**1**-d22) = -1210.645722 Hartree.

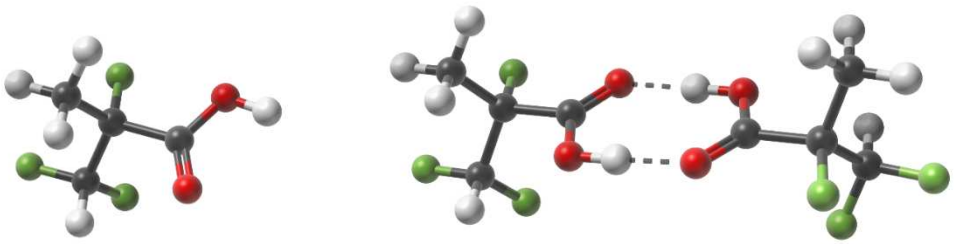

Figure 2. Structures of the **1** monomer and dimer in their lowest energy ($\Delta H°$) conformers **1**-m1 (left) and **1**-d22 (right) as calculated at the M06-2X / 6-311++G(2d,p) / SCRF($CHCl_3$) level of theory.

The fingerprint regions (i.e. 950–1600 cm^{-1}) of the calculated **1** monomer and dimer IR and VCD spectra are shown in Figure 3, together with the experimental spectra. The calculated **1** monomer and dimer spectra show some distinct features, most notably the red shift of the carbonyl stretch vibration at 1750 cm^{-1} in the IR spectra and the region 1400–1500 cm^{-1} in the VCD spectra when moving from the monomer to the dimer spectra. Comparing these regions with the corresponding regions in the experimental IR and VCD spectra suggests that a combination of both monomer and dimer spectra is needed to optimally match the experimentally observed spectra. The monomer:dimer ratio was estimated by calculating the overlap integral in the wavenumber range 950–1600 cm^{-1} between the experimental spectrum and a calculated spectrum consisting of various monomer and dimer spectral contributions (0:100% to 100:0% in increments of 5%), as illustrated in Figure 4.

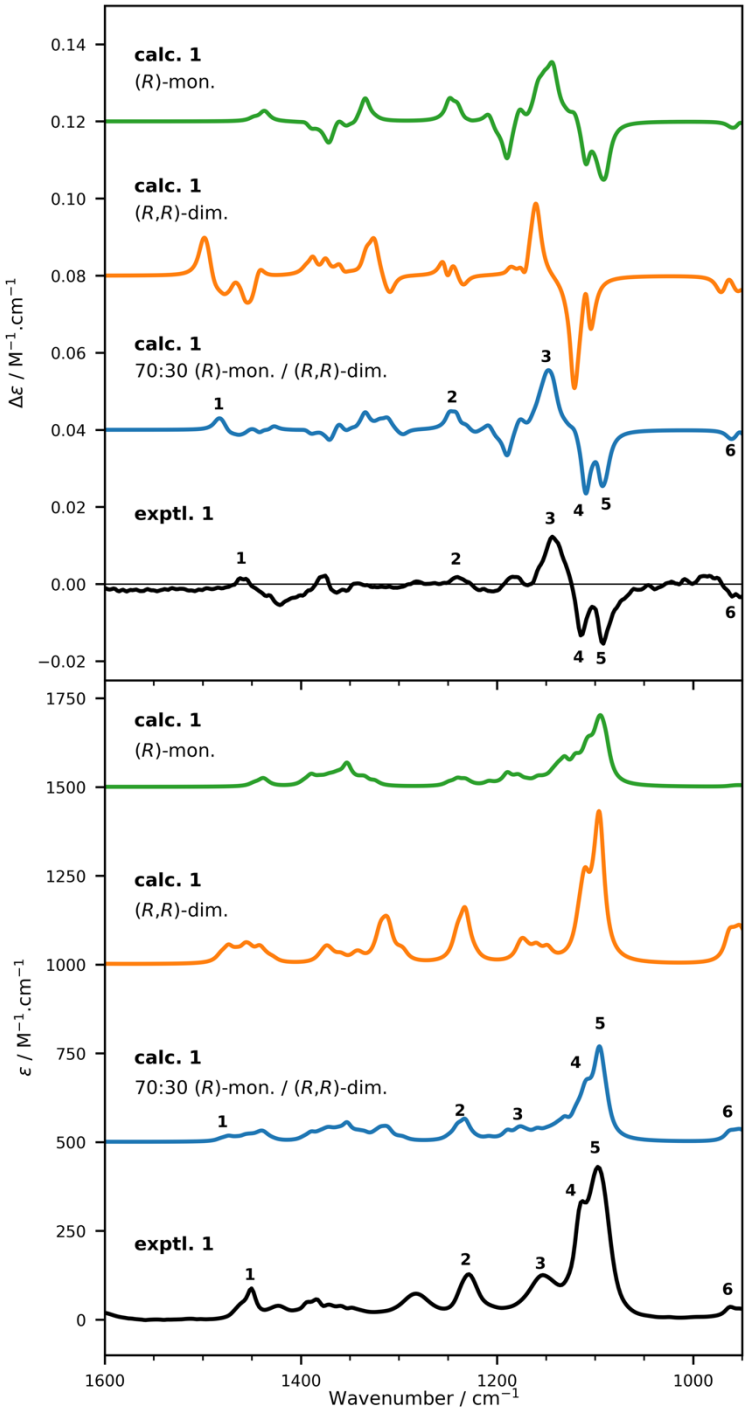

Figure 3. Comparison of the experimental VCD (top) and IR (bottom) spectra (black) of compound **1** with the calculated monomer:dimer combinations (blue) of the calculated spectra of its (*R*)-monomer conformations (green) and (*R*,*R*)-dimers conformations (orange). The VCD spectrum was obtained via the virtual racemate. Consequently, the experimental IR and VCD spectra presented are displayed as ½ of [**1B** + **1A**] and ½ of [**1B** - **1A**], respectively. The calculated line spectra were frequency-scaled with a factor of 0.967 to match the experimental spectra. For clarity, the VCD and IR spectra are offset by 0.04 and 500 $M^{-1}\cdot cm^{-1}$, respectively. Numbers denote band assignments.

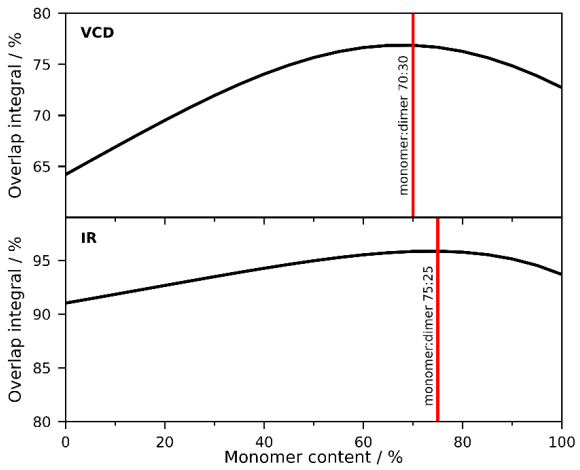

Figure 4. The overlap integral between the experimental VCD and IR spectra of **1** and the calculated VCD and IR spectra, respectively, with different **1** monomer:dimer ratios. Red lines indicate the monomer:dimer ratio resulting in the highest overlap between calculation and experiment.

Independently of the use of the IR or the VCD spectrum, a very similar monomer:dimer ratio was found. The monomer:dimer ratio was estimated to be 75:25 with an overlap integral of 95.9% for IR and 70:30 with an overlap integral of 76.9% for VCD. As shown in Figure 4, the VCD overlap integral is more sensitive to changes in this ratio, therefore a monomer:dimer ratio of 70:30 was used for both IR and VCD, resulting in the calculated ratio spectra presented in Figure 3. The experimental VCD spectrum of **1,** obtained via the virtual racemate and thus displayed as ½ [**1B** - **1A**], is in good agreement with this calculated ratio spectrum, as indicated by band assignments 1–6. Based on the clear +/-/- pattern of band assignments 3–5 arising from the C−F asymmetric and symmetric stretching vibrations, together with the high value of the VCD overlap integral, it can be concluded that sample **1A** is (*S*)-2,3,3-trifluoro-2-methylpropanoic acid and **1B** is (*R*)-2,3,3-trifluoro-2-methylpropanoic acid.

For completeness, a similar analysis was performed with the more commonly used B3LYP functional, with and without Grimme dispersion correction (GD3).[34] A comparison of the experimental and calculated (B3LYP and B3LYP-GD3) VCD and IR spectra of compound **1** is included in the ESI. At the B3LYP / 6-311++G(2d,p) / SCRF($CHCl_3$) level of theory and using a scaling factor of 1.012, the **1** monomer:dimer ratio was estimated to be 95:5 with an overlap integral of 61.0% for IR and 90:10 with an overlap integral of 62.1% for VCD. As discussed by Kreienborg *et al.*[57], the harmonic frequency calculations of the C−F asymmetric and symmetric stretching vibrations were significantly improved

when the M06-2X functional was used. This is most evident from the previously discussed +/-/- pattern (bands 3–5), which is still present in the B3LYP ratio spectrum, but with a mismatch in harmonic frequencies, resulting in an overall lower overlap integral and a significantly different monomer:dimer ratio. This mismatch, however, does not alter the aforementioned assignments. The inclusion of dispersion correction (GD3) when using B3LYP did not improve the predicted spectral pattern.

In the case of compound **2**, a conformational analysis via the same methodology as described above resulted in three unique conformations of the **2** (*R*)-monomer, of which two *cis*, and three corresponding **2** (*R*,*R*)-dimer complexes. The lowest-energy conformers of the **2** monomer (left) and dimer (right) are displayed in Figure 5. The torsional angles, associated enthalpy-corrected energies and corresponding Boltzmann populations of the **2** monomer and dimer conformers are summarized in the ESI. The fingerprint regions of the calculated and experimental VCD and IR spectra of **2** are shown in Figure 6, with the VCD spectrum displayed as ½ [**2A** - **2B**].

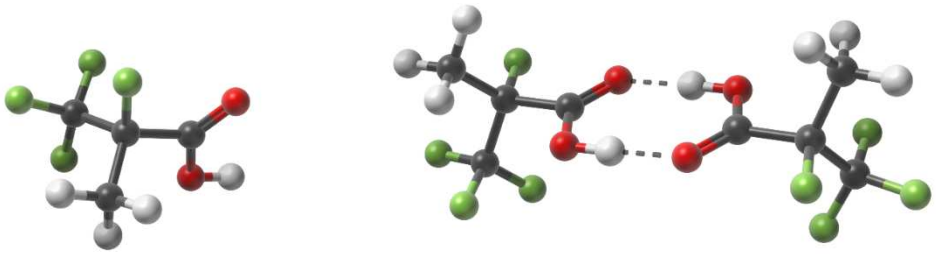

Figure 5. Structures of the **2** monomer and dimer in their lowest energy ($\Delta H°$) conformers **2**-m1 (left) and **2**-d11 (right) as calculated at the M06-2X / 6-311++G(2d,p) / SCRF($CHCl_3$) level of theory.

The monomer:dimer ratio of **2** was estimated to be 85:15 with an overlap integral of 90.2% for IR, and 75:25 with an overlap integral of 42.9% for VCD, using a scaling factor of 0.975. Similar analyses using the B3LYP functional with and without dispersion correction, included in the ESI, again did not improve the spectral pattern. Based on conservative band assignments 1–4, it can be concluded that sample **2A** is (*R*)-2,3,3,3-tetrafluoro-2-methylpropionic acid and **2B** is (*S*)-2,3,3,3-tetrafluoro-2-methylpropionic acid. Nonetheless, the agreement between experiment and calculations for the AC determination of **2** is in general less convincing than in the case of **1**, as exemplified by the much lower value of the VCD overlap integral. Hence, it provides an excellent opportunity for a similar AC analysis through MRR spectroscopy.

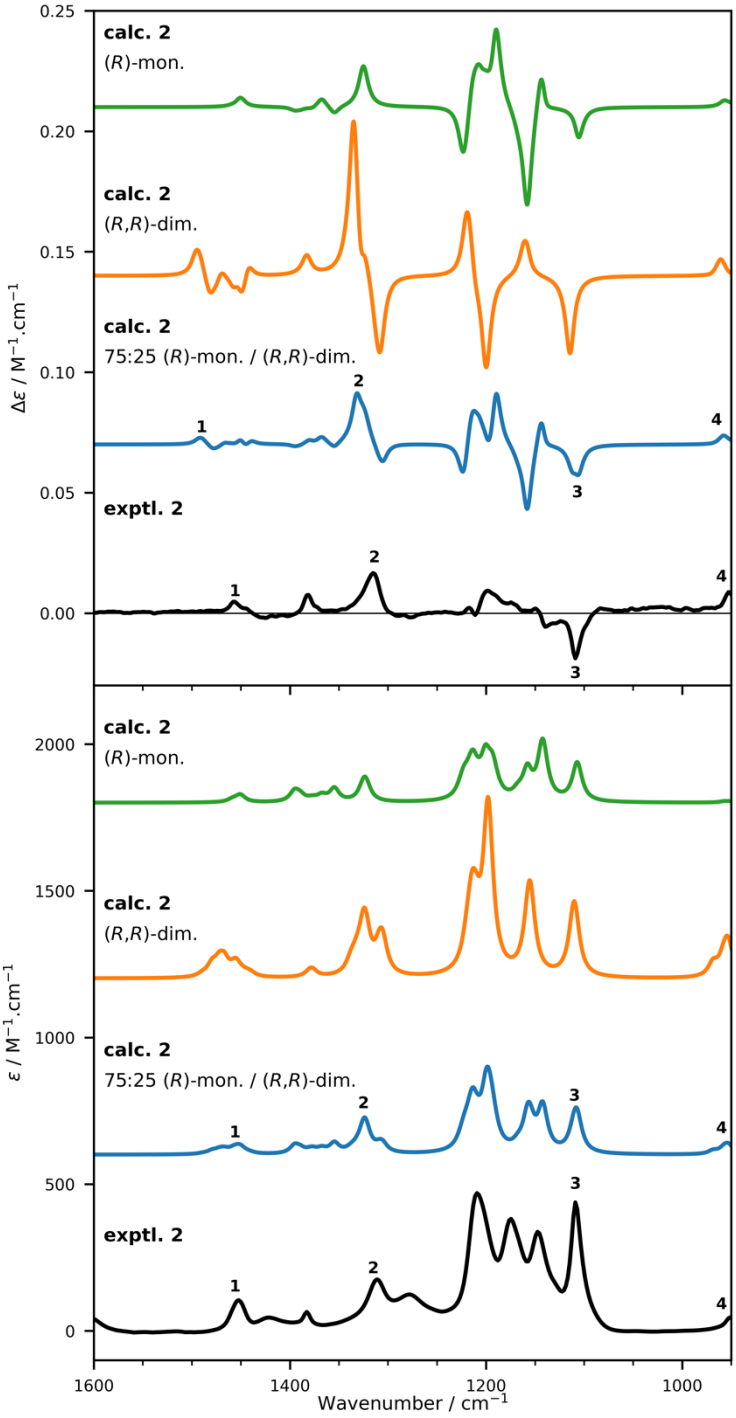

Figure 6. Comparison of the experimental VCD (top) and IR (bottom) spectra (black) of compound **2** with the calculated monomer:dimer combinations (blue) of the calculated spectra of its (*R*)-monomers conformations (green) and (*R*,*R*)-dimers conformations (orange). The VCD spectrum was obtained via the virtual racemate. Consequently, the experimental IR and VCD spectra presented are displayed as ½ of [**2A** + **2B**] and ½ of [**2A** - **2B**], respectively. The calculated line spectra were frequency-scaled with a factor of 0.975 to match the experimental spectra. For clarity, the VCD and IR spectra are offset by 0.07 and 600 $M^{-1}\cdot cm^{-1}$, respectively. Numbers denote band assignments.

3.2 Rotational analysis

The first step in performing a chiral tagging analysis using MRR is to determine the optimal chiral tag. The primary consideration is selecting a tag that results in non-covalent complexes with the greatest sensitivity. For the determination of AC, another key consideration is that the relative stereochemistry of the complexes must be unambiguously identified by correlation to quantum chemistry calculations. Both propylene oxide (PO) and 1,1,1-trifluoropropan-2-ol (TFIP) were assessed as the carboxylic acid group of **1** and **2** can act as both an H-bond donor and H-bond receptor. For both **1** and **2**, PO yielded complexes with the greatest sensitivity and so these measurements were analyzed first for AC determination.

The spectrum of **1** was measured in the presence of racemic PO and enantiopure (*S*)-PO. Example spectra are shown in the ESI. Two strong complexes (Assignments 1 and 2) were assigned in the measurement of **1** with racemic PO (see Tables 3 and 4). These two assignments account for all of the strongest transitions in the isolated tag spectrum (i.e. the measured spectrum with all the transitions related to the analyte and tag monomer removed). Only Assignment 2 was detected in the measurement of **1A** with enantiopure PO, while only Assignment 1 was detected in the measurement of **1B** with (*S*)-PO, which confirms that the two assignments arise from complexes with opposite stereochemistry.

Table 3. Comparison of experimental Assignment 1 of compound **1** with calculated isomers of compound 1 complexed with propylene oxide that are a match based on rotational constants. The relative dipole moment and relative energy of the stereoisomer are presented for each isomer. Isomers were calculated at B3LYP-GD3BJ / def2-TZVP level of theory. Full details of the spectroscopic fit and a summary of the quantum chemistry calculations can be found in the ESI.

	Assignment 1 (Experimental)	Homochiral Isomer 4 (Calculated)	Heterochiral Isomer 1 (Calculated)
A (MHz)	1586.740	1584.33 (+0.15%)	1580.10 (+0.42%)
B (MHz)	335.37136	333.22 (+0.64%)	335.19 (+0.05%)
C (MHz)	316.91203	314.42 (+0.79%)	316.57 (+0.11%)
$\mu_a^2 : \mu_b^2 : \mu_c^2$	1.00 : 0.00 : 0.00	1.00 : 0.01 : 0.00	1.00 : 0.00 : 0.06
ΔE (kJ/mol)		1.80	0.00

Table 4. Comparison of experimental Assignment 2 of compound **1** with calculated isomers of compound 1 complexed with propylene oxide that are a match based on rotational constants. The relative dipole moment and relative energy of the stereoisomer are presented for each isomer. Isomers were calculated at B3LYP-GD3BJ / def2-TZVP level of theory. Full details of the spectroscopic fit and a summary of the quantum chemistry calculations can be found in the ESI.

	Assignment 2 (Experimental)	Homochiral Isomer 1 (Calculated)	Homochiral Isomer 3 (Calculated)	Heterochiral Isomer 3 (Calculated)
A (MHz)	1729.620	1723.64 (+0.35%)	1726.28 (+0.19%)	1720.31 (+0.54%)
B (MHz)	322.98647	322.65 (+0.10%)	320.97 (+0.62%)	320.54 (+0.76%)
C (MHz)	310.81498	310.43 (+0.12%)	309.98 (+0.27)	309.56 (+0.40%)
$\mu_a^2 : \mu_b^2 : \mu_c^2$	1.00 : 0.00 : 0.00	1.00 : 0.00 : 0.06	1.00 : 0.02 : 0.49	1.00 : 0.01 : 0.00
ΔE (kJ/mol)		0.0	0.80	1.87

The structural information that is derived from MRR assignments includes the rotational constants *A*, *B*, and *C* (which are inversely proportional to the three moments of inertia in the molecule's principal axis system), and the direction of the dipole moment, which is determined from the relative intensities of transitions with *a*, *b*, and *c*-type selection rules. In general, a "match" with theory for non-covalent complexes at the level of theory used in this paper requires that all three rotational constants agree within 2.5%. The rotational constants and squared dipole components of Assignments 1 and 2 as well as the calculated rotational constants and squared dipole components of the homo- and heterochiral complex isomers are presented in Tables 3 and 4, respectively. Figure 7 shows the rotational constants comparison of the two strong experimental assignments with the low-energy isomers of both homochiral and heterochiral complex geometries. The terms heterochiral and homochiral refer to the relative stereochemistry of the chiral tag and analyte based on the Cahn-Ingold-Prelog naming convention. For both assignments, there are calculated structures with each stereochemistry where the rotational constants match is acceptable. Assignment 1 agrees well with Heterochiral Isomer 1 (the heterochiral complex with lowest calculated energy), while Assignment 2 agrees well with Homochiral Isomer 1. However, on the basis of the MRR parameters, Assignment 1 also agrees with Homochiral Isomer 4, while Assignment 2 also agrees with Heterochiral Isomer 3, which would flip the resulting AC assignment. However, the higher energy of these isomers (1.8–1.9 kJ mol^{-1}) makes this assignment less likely. From Figure 7, it can also be seen that Assignment 2 could also be matched to Homochiral Isomer 3 based on the rotational constants; however, the dipole moment direction contradicts this analysis, as *c*-type transitions would be predicted at considerable strength and these are not detected experimentally.

While the calculated energy of the isomers already suggests that Assignment 1 is heterochiral and Assignment 2 is homochiral, it is possible to obtain additional confirmatory information from the same spectrum through the identification of other complex geometries. The additional isomers are higher in energy and, consequently, the intensity of the spectra is weaker than the lowest-energy isomers assigned in the racemic measurement. Three additional isomers were assigned in the enantiopure measurements of **1A** and **1B**. Of the three assignments (labeled Assignment 3–5), two have the same relative stereochemistry as Assignment 2 and one assignment has the same relative stereochemistry as Assignment 1 based on the measurements with enantiopure PO. The stereochemistry of the higher-energy isomers was assigned by comparison with the calculated structures and is presented in the ESI. This comparison showed that Assignment 3 and Assignment 4 are homochiral and Assignment 5 is heterochiral. These assignments confirm the AC analysis, i.e. that Assignment 1 is heterochiral and Assignment 2 is homochiral. Since (*S*)-PO was used as the tag, this allows the AC of **1A** to be confirmed as (*S*)-2,3,3-trifluoro-2-methylpropanoic acid, and that of **1B** as (*R*)-2,3,3-trifluoro-2-methylpropanoic acid.

For compound **2**, again PO was found to generate chiral tag complexes with the strongest intensity, and a total of four complexes (two with each stereochemistry) were assigned. However, the MRR parameters of the heterochiral and homochiral tag complexes of **2** with PO were too similar in both rotational constants and isomer energies to enable stereochemical identification. Therefore, the spectrum of **2** with TFIP was used for the AC assignment. Three spectral assignments were made in the measurement of **2** with racemic TFIP. While Assignments 1 and 2 have plausible matches to either homochiral or heterochiral complex geometries, Assignment 3 is unambiguously identified as a heterochiral complex. This assignment was present in the measurement of **2A** with enantiopure (*S*)-TFIP, so it was assigned as (*R*)-2,3,3,3-tetrafluoro-2-methylpropanoic acid, and **2B** was assigned as (*S*)-2,3,3,3-tetrafluoro-2-methylpropionic acid. A complete summary of the quantum chemistry and spectral assignments with both PO and TFIP can be found in the ESI.

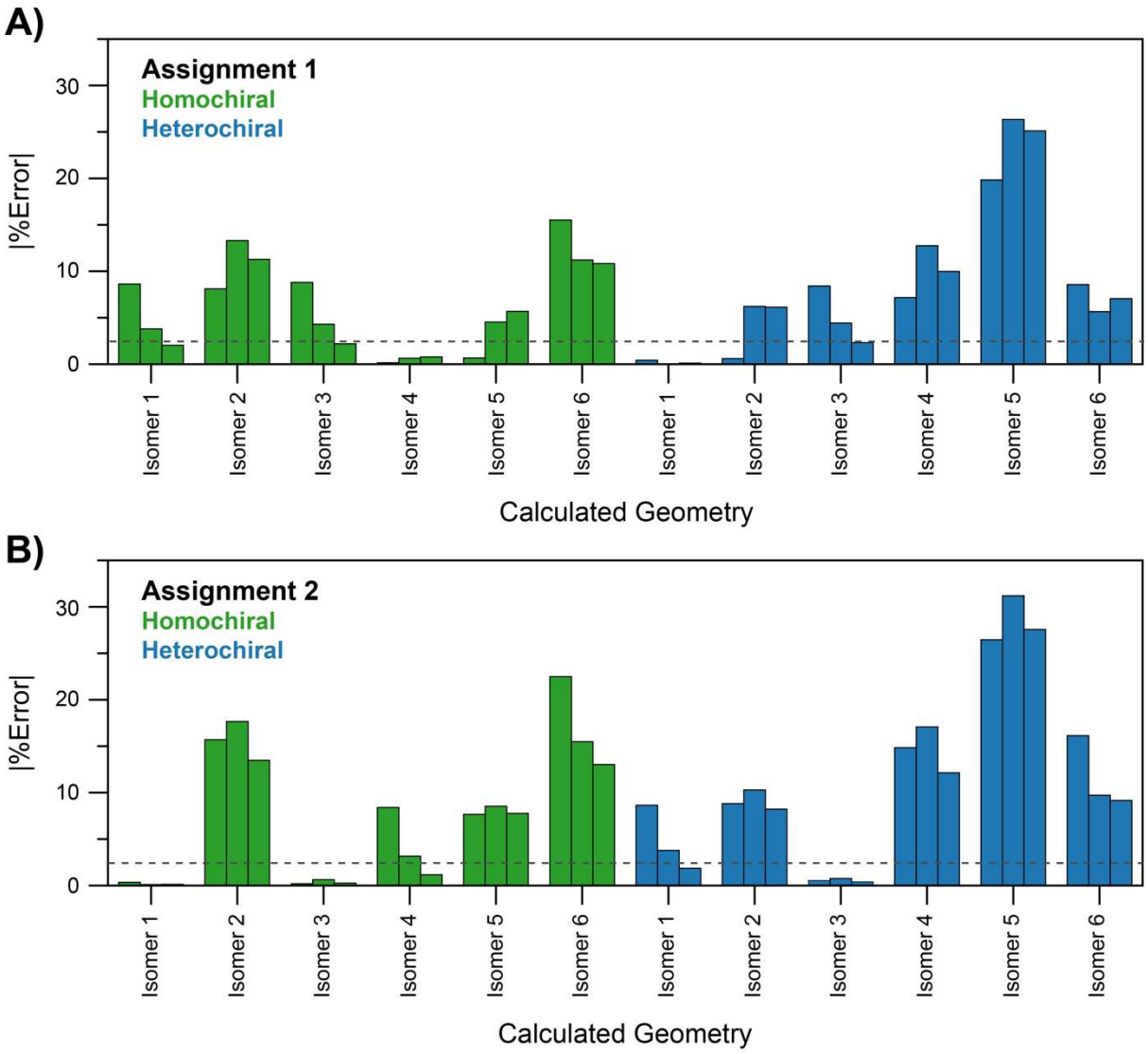

Figure 7. Rotational constants comparison of experimental spectral assignments from measurement of **1** with racemic PO with calculated low-energy homochiral and heterochiral isomers. The magnitude %error in rotational constants A, B, and C is presented. The dashed line indicates the accepted level of %error in constants for a "match." (A) Two geometries are a "match" with Assignment 1 based on the criteria of rotational constant agreement: Homochiral Isomer 4 and Heterochiral Isomer 1. (B) Three geometries have rotational constants within 2.5% of Assignment 2: Homochiral Isomer 1, Homochiral Isomer 3, and Heterochiral Isomer 3. All isomers were calculated at B3LYP-GD3BJ / def2-TZVP level of theory.

4 Conclusion

In this work, the ACs of 2,3,3-trifluoro-2-methylpropanoic acid (**1**) and 2,3,3,3-tetrafluoro-2-methylpropanoic acid (**2**) were unambiguously and independently determined via VCD and MRR spectroscopy.

In the case of VCD, it is imperative to account for all conformers, as VCD spectra are inherently influenced by the Boltzmann contributions of each individual conformer and AC assignment is based on the similarity of experimental and calculated spectra. Specifically for carboxylic acids, this requires accounting for conformers of both monomers and dimers. The M06-2X functional was shown to be the superior functional over B3LYP, with or without dispersion correction, for prediction of the C–F normal modes, which is in line with recent findings in literature.[57] The AC of **1** could be assigned with high confidence, but the AC of **2** proved to be less convincing, as illustrated by the lower overlap integral values. When AC assignment via VCD suffers from some uncertainty, as was the case with **2**, MRR offers much added value.

In the case of MRR, individual (low-energy) isomers can be distinguished in the spectrum, removing the need to account for all possible geometries, as is the case in VCD. Assignment of calculated isomers to spectral fits allows for rapid determination of the AC through the comparison of rotational constants. Isomer energies also aid in this regard, as they have generally shown to be very accurate in predicting the isomers that are most likely to be experimentally detected. It should be noted that, in contrast to prior studies where AC has been determined by MRR, most of the assigned geometries in the spectra had more than one plausible computational match, requiring more information to make unambiguous identifications. Due to their small molecular weight and highly fluorinated nature, **1** and **2** were shown to interact with the tags almost exclusively through the carboxylic acid moiety and to lack the secondary stabilizing interactions that commonly appear with other analytes. Consequently, multiple isomers with similar energy and geometry are possible. Nevertheless, the use of multiple tags and isomeric structures in the assignment, as well as the high accuracy of the computational chemistry on both the geometry and relative isomer energy, provides MRR with the capability to accurately determine AC in these cases. MRR can also be used to determine the enantiomeric excess of samples, enabling complete chiral analysis in a single measurement.

Thanks to the pioneering work of L. A. Nafie, to whom this work is dedicated, VCD has established itself over the past decades as a reliable method to quickly and unambiguously determine the AC of APIs, leading to its inclusion in the European and U.S. pharmacopeias.[72] It is the authors' hope that this comparative study showcases not only the strength and beauty of contemporary VCD analysis, but also the potential of MRR spectroscopy and its unique contributions to the analytical toolbox.

Acknowledgements

Flanders Innovation & Entrepreneurship (VLAIO – HBC.2021.0795) is acknowledged for offering financial support. The Flemish Supercomputing Centre (VSC) is also acknowledged for providing computational resources and support.

Conflicts of interest

R.E.S. and J.L.N. have equity in BrightSpec, Inc. The authors declare no other conflicts of interest.

Author contributions

Conceptualization: D.J.S.D.W., S.L., J.B., W.H.; Methodology: D.J.S.D.W, S.L, J.B., R.E.S., J.L.N.; Validation: D.J.S.D.W., S.L., J.B., R.E.S.; Formal analysis: D.J.S.D.W., S.L., J.B., R.E.S.; Investigation: D.J.S.D.W., S.L., J.B., R.E.S.; Resources: W.H., J.L.N., P.V.; Data Curation: J.B., J.L.N.; Writing - Original Draft: D.J.S.D.W., S.L., J.B., R.E.S.; Writing - Review & Editing: D.J.S.D.W., S.L., R.E.S., J.B., J.L.N., K.G., M.B., N.V., W.H.; Visualization: D.J.S.D.W., S.L., R.E.S.; Supervision: J.L.N., K.G., N.V., W.H.; Project administration: J.B., R.E.S.; Funding acquisition: J.B., N.V., W.H.; All authors have read and agreed to the published version of the manuscript.

5 References

[1] H. Alkadi and R. Jbeily, *Infectious Disorders - Drug Targets*, 2018, **18**, 88-95.
[2] J. Ceramella, D. Iacopetta, A. Franchini, M. De Luca, C. Saturnino, I. Andreu, M. S. Sinicropi and A. Catalano, *Applied Sciences*, 2022, **12**, 10909.
[3] S. A. Biyani, Y. W. Moriuchi and D. H. Thompson, *Chemistry–Methods*, 2021, **1**, 323-339.
[4] A. L. Albright and J. M. White, in *Metabolomics Tools for Natural Product Discovery: Methods and Protocols*, eds. U. Roessner and D. Dias, Humana Press, Totowa, New Jersey, U.S.A., 2013, pp. 149-162.
[5] L.-Y. Kong and P. Wang, *Chinese Journal of Natural Medicines*, 2013, **11**, 193-198.
[6] Z. Wang, L. Zhao, Y. Chen, W. Xu and T. Sun, *European Journal of Organic Chemistry*, 2014, **2014**, 3814-3821.
[7] F. Faigl, B. Vas-Feldhoffer, M. Kubinyi, K. Pál, G. Tárkányi and M. Czugler, *Tetrahedron: Asymmetry*, 2009, **20**, 98-103.
[8] N. Berova, P. L. Polavarapu, K. Nakanishi and R. W. Woody, *Comprehensive Chiroptical Spectroscopy, Volume 1: Instrumentation, Methodologies, and Theoretical Simulations*, Wiley, Hoboken, New Jersey, U.S.A., 2011.
[9] P. J. Stephens, F. J. Devlin, J. R. Cheeseman, M. J. Frisch, O. Bortolini and P. Besse, *Chirality*, 2003, **15**, S57-S64.
[10] J. A. Dale and H. S. Mosher, *Journal of the American Chemical Society*, 1973, **95**, 512-519.
[11] T. R. Hoye, C. S. Jeffrey and F. Shao, *Nature Protocols*, 2007, **2**, 2451-2458.
[12] Y. He, W. Bo, R. K. Dukor and L. A. Nafie, *Applied Spectroscopy*, 2011, **65**, 699-723.

[13] C. Merten, T. P. Golub and N. M. Kreienborg, *The Journal of Organic Chemistry*, 2019, **84**, 8797-8814.
[14] T. Brotin, N. Daugey, N. Vanthuyne, E. Jeanneau, L. Ducasse and T. Buffeteau, *The Journal of Physical Chemistry B*, 2015, **119**, 8631-8639.
[15] D. P. Demarque, S. Heinrich, F. Schulz and C. Merten, *Chemical Communications*, 2020, **56**, 10926-10929.
[16] J. Bogaerts, F. Desmet, R. Aerts, P. W. E. Bultinck, W. Herrebout and C. Johannessen, *Physical Chemistry Chemical Physics*, 2020, **22**, 18014-18024.
[17] L. A. Nafie, *Vibrational Optical Activity: Principles and Applications*, Wiley, Chichester, West Sussex, U.K., 2011.
[18] P. J. Stephens, F. J. Devlin and J. R. Cheeseman, *VCD Spectroscopy for Organic Chemists*, CRC Press, Boca Raton, Florida, U.S.A., 2012.
[19] P. J. Stephens, *The Journal of Physical Chemistry*, 1985, **89**, 748-752.
[20] R. E. Sonstrom, J. L. Neill, A. V. Mikhonin, R. Doetzer and B. H. Pate, *Chirality*, 2022, **34**, 114-125.
[21] M. D. Mills, R. E. Sonstrom, Z. P. Vang, J. L. Neill, H. N. Scolati, C. T. West, B. H. Pate and J. R. Clark, *Angewandte Chemie International Edition*, 2022, **61**, e202207275.
[22] S. R. Domingos, C. Pérez, M. D. Marshall, H. O. Leung and M. Schnell, *Chemical Science*, 2020, **11**, 10863-10870.
[23] S. R. Domingos, A. Cnossen, W. J. Buma, W. R. Browne, B. L. Feringa and M. Schnell, *Angewandte Chemie International Edition*, 2017, **56**, 11209-11212.
[24] W. Gordy and R. L. Cook, *Microwave Molecular Spectra*, Wiley, New York, U.S.A., 1984.
[25] L. Evangelisti, K. J. Mayer, M. S. Holdren, T. Smart, C. West, B. Pate, G. Sedo, F. E. Marshall and G. S. Grubbs, II, *Chiral Tagging of Verbenone with 3-butyn-2-ol for Establishing Absolute Configuration and Determining Enantiomeric Excess*, 72nd International Symposium on Molecular Spectroscopy, 2017.
[26] B. H. Pate, L. Evangelisti, W. Caminati, Y. Xu, J. Thomas, D. Patterson, C. Perez and M. Schnell, in *Chiral Analysis (Second Edition)*, ed. P. L. Polavarapu, Elsevier, 2018, pp. 679-729.
[27] K. Mayer, C. West, F. E. Marshall, G. Sedo, G. S. Grubbs, L. Evangelisti and B. H. Pate, *Physical Chemistry Chemical Physics*, 2022, **24**, 27705-27721.
[28] R. D. Suenram, J. U. Grabow, A. Zuban and I. Leonov, *Review of Scientific Instruments*, 1999, **70**, 2127-2135.
[29] T. J. Balle and W. H. Flygare, *Review of Scientific Instruments*, 1981, **52**, 33-45.
[30] G. G. Brown, B. C. Dian, K. O. Douglass, S. M. Geyer, S. T. Shipman and B. H. Pate, *Review of Scientific Instruments*, 2008, **79**, 053103.
[31] S. Grimme, S. Ehrlich and L. Goerigk, *Journal of Computational Chemistry*, 2011, **32**, 1456-1465.
[32] P. Pracht, F. Bohle and S. Grimme, *Physical Chemistry Chemical Physics*, 2020, **22**, 7169-7192.
[33] F. Weigend and R. Ahlrichs, *Physical Chemistry Chemical Physics*, 2005, **7**, 3297.
[34] S. Grimme, J. Antony, S. Ehrlich and H. Krieg, *The Journal of Chemical Physics*, 2010, **132**.
[35] J. L. Neill, A. V. Mikhonin, T. Chen, R. E. Sonstrom and B. H. Pate, *Journal of Pharmaceutical and Biomedical Analysis*, 2020, **189**, 113474.
[36] R. E. Sonstrom, D. M. Cannon and J. L. Neill, *Symmetry*, 2022, **14**, 917.
[37] J. L. Neill, Y. Yang, M. T. Muckle, R. L. Reynolds, L. Evangelisti, R. E. Sonstrom, B. H. Pate and B. F. Gupton, *Organic Process Research & Development*, 2019, **23**, 1046-1051.
[38] L. A. Joyce, D. M. Schultz, E. C. Sherer, J. L. Neill, R. E. Sonstrom and B. H. Pate, *Chemical Science*, 2020, **11**, 6332-6338.
[39] Z. P. Vang, A. Reyes, R. E. Sonstrom, M. S. Holdren, S. E. Sloane, I. Y. Alansari, J. L. Neill, B. H. Pate and J. R. Clark, *Journal of the American Chemical Society*, 2021, **143**, 7707-7718.
[40] P. L. Polavarapu, *Chiral Analysis: Advances in Spectroscopy, Chromatography and Emerging Methods*, Elsevier Science, Amsterdam, Netherlands, 2018.

[41] N. A. McGrath, M. Brichacek and J. T. Njardarson, *Journal of Chemical Education*, 2010, **87**, 1348-1349.
[42] R. E. Williams and C. M. Marshall, *Top 200 Pharmaceuticals by Retail Sales in 2022*, [*], (accessed on June 13th, 2023).
[43] K. Bünnemann and C. Merten, *Physical Chemistry Chemical Physics*, 2017, **19**, 18948-18956.
[44] K. Bünnemann, C. H. Pollok and C. Merten, *The Journal of Physical Chemistry B*, 2018, **122**, 8056-8064.
[45] S. Patai, *The Chemistry of Acid Derivatives, Supplement B, Volume 2, Parts 1 and 2*, Wiley, Chichester, West Sussex, U.K., 1992.
[46] P. A. Kollman and L. C. Allen, *Chemical Reviews*, 1972, **72**, 283-303.
[47] A. D. Becke, *The Journal of Chemical Physics*, 1993, **98**, 5648-5652.
[48] C. Lee, W. Yang and R. G. Parr, *Physical Review B*, 1988, **37**, 785-789.
[49] S. H. Vosko, L. Wilk and M. Nusair, *Canadian Journal of Physics*, 1980, **58**, 1200-1211.
[50] P. J. Stephens, F. J. Devlin, C. F. Chabalowski and M. J. Frisch, *The Journal of Physical Chemistry*, 1994, **98**, 11623-11627.
[51] A. D. Becke, *Physical Review A*, 1988, **38**, 3098-3100.
[52] J. P. Perdew, *Electronic Structure of Solids '91*, 1991, **17**, 11-20.
[53] J. P. Perdew, J. A. Chevary, S. H. Vosko, K. A. Jackson, M. R. Pederson, D. J. Singh and C. Fiolhais, *Physical Review B*, 1992, **46**, 6671-6687.
[54] J. P. Perdew, J. A. Chevary, S. H. Vosko, K. A. Jackson, M. R. Pederson, D. J. Singh and C. Fiolhais, *Physical Review B*, 1993, **48**, 4978-4978.
[55] J. P. Perdew, K. Burke and Y. Wang, *Physical Review B*, 1996, **54**, 16533-16539.
[56] K. Burke, J. P. Perdew and Y. Wang, in *Electronic Density Functional Theory: Recent Progress and New Directions*, eds. J. F. Dobson, G. Vignale and M. P. Das, Springer US, Boston, Massachussetts, 1998, pp. 81-111.
[57] N. M. Kreienborg and C. Merten, *Physical Chemistry Chemical Physics*, 2019, **21**, 3506-3511.
[58] Y. Zhao and D. G. Truhlar, *Theoretical Chemistry Accounts*, 2008, **120**, 215-241.
[59] K. E. Gilbert and M. M. Midland, *PCModel Version 10.07*, Bloomington, Indiana, U.S.A., 2020.
[60] T. A. Halgren, *Journal of Computational Chemistry*, 1999, **20**, 720-729.
[61] M. J. Frisch, G. W. Trucks, H. B. Schlegel, G. E. Scuseria, M. A. Robb, J. R. Cheeseman, G. Scalmani, V. Barone, G. A. Petersson, H. Nakatsuji, X. Li, M. Caricato, A. V. Marenich, J. Bloino, B. G. Janesko, R. Gomperts, B. Mennucci, H. P. Hratchian, J. V. Ortiz, A. F. Izmaylov, J. L. Sonnenberg, Williams, F. Ding, F. Lipparini, F. Egidi, J. Goings, B. Peng, A. Petrone, T. Henderson, D. Ranasinghe, V. G. Zakrzewski, J. Gao, N. Rega, G. Zheng, W. Liang, M. Hada, M. Ehara, K. Toyota, R. Fukuda, J. Hasegawa, M. Ishida, T. Nakajima, Y. Honda, O. Kitao, H. Nakai, T. Vreven, K. Throssell, J. A. Montgomery Jr., J. E. Peralta, F. Ogliaro, M. J. Bearpark, J. J. Heyd, E. N. Brothers, K. N. Kudin, V. N. Staroverov, T. A. Keith, R. Kobayashi, J. Normand, K. Raghavachari, A. P. Rendell, J. C. Burant, S. S. Iyengar, J. Tomasi, M. Cossi, J. M. Millam, M. Klene, C. Adamo, R. Cammi, J. W. Ochterski, R. L. Martin, K. Morokuma, O. Farkas, J. B. Foresman and D. J. Fox, *Gaussian 16 Rev. C.01*, Gaussian 16 Rev. C.01, Wallingford, Connecticut, U.S.A., 2016.
[62] Y. Zhao and D. G. Truhlar, *Accounts of Chemical Research*, 2008, **41**, 157-167.
[63] T. Clark, J. Chandrasekhar, G. W. Spitznagel and P. V. R. Schleyer, *Journal of Computational Chemistry*, 1983, **4**, 294-301.
[64] K. L. Schuchardt, B. T. Didier, T. Elsethagen, L. Sun, V. Gurumoorthi, J. Chase, J. Li and T. L. Windus, *Journal of Chemical Information and Modeling*, 2007, **47**, 1045-1052.
[65] D. Feller, *Journal of Computational Chemistry*, 1996, **17**, 1571-1586.
[66] R. Krishnan, J. S. Binkley, R. Seeger and J. A. Pople, *The Journal of Chemical Physics*, 1980, **72**, 650-654.
[67] B. P. Pritchard, D. Altarawy, B. Didier, T. D. Gibsom and T. L. Windus, *Journal of Chemical Information and Modeling*, 2019, **59**, 4814-4820.

[68] S. Miertuš, E. Scrocco and J. Tomasi, *Chemical Physics*, 1981, **55**, 117-129.
[69] S. Miertuš and J. Tomasi, *Chemical Physics*, 1982, **65**, 239-245.
[70] J.-L. Pascual-ahuir, E. Silla and I. Tunon, *Journal of Computational Chemistry*, 1994, **15**, 1127-1138.
[71] C. Mensch, L. D. Barron and C. Johannessen, *Physical Chemistry Chemical Physics*, 2016, **18**, 31757-31768.
[72] L. Nafie, O. McConnel, D. Minick, E. Kellenbach, Y. He, B. Wang, R. Dukor, M. Bartberger and H. Pappa, *Pharmacopeial Forum*, 2013, **39**, 311-452.